

Wavelength-scale Optical Parametric Oscillators

Saman Jahani,¹ Arkadev Roy,¹ and Alireza Marandi^{1,*}

¹*Department of Electrical Engineering, California Institute of Technology, Pasadena, CA 91125, USA.*
(Dated: April 30, 2020)

Despite recent progress in nonlinear conversion in wavelength-scale resonators, there are still open questions on the possibility of parametric down-conversion and oscillation in such resonators. The existing theories have limitations in accurately predicting the behaviors of wavelength-scale nonlinear resonators, especially where multiple resonances are involved. We present a general approach to predict the behavior and estimate the oscillation threshold of multi-mode wavelength-scale optical parametric oscillators (OPOs). As an example, we propose an OPO based on Mie-type multipolar resonances, and we demonstrate that due to the nonlinear interaction between the multipolar modes, the OPO threshold, compared to the single-mode case, can be reduced by a factor which is significantly larger than the number of interacting modes. We compare the threshold for electric and magnetic mode excitations to emphasise the importance of the field overlap, the phase matching counterpart in wavelength-scale resonators. We establish an explicit connection between the second-harmonic generation efficiency and the OPO threshold. This allows us to estimate the OPO threshold based on measured or simulated second-harmonic generation in different class of resonators, such as bound-state in the continuum and inversely designed resonators. Our approach for analyzing and modeling miniaturized OPOs can open unprecedented opportunities for classical and quantum nonlinear photonics.

I. INTRODUCTION

Optical parametric oscillators (OPOs) have been widely used for many applications ranging from metrology and spectroscopy to quantum information science [1–9]. OPOs consist of a medium with quadratic or Kerr nonlinearity within a resonator, which is typically much larger than the operation wavelength, converting pump photons to signal and idler photons [2–7]. At degeneracy, the indistinguishable signal and idler of an OPO can form a squeezed vacuum state below the oscillation threshold [10, 11] that have been used for several applications in quantum information processing [9, 12–14]. Above threshold, the conversion efficiency boosts rapidly and the output signal illustrates a binary phase state which can be utilized as a spin in an artificial Ising network [15, 16]. Above-threshold degenerate OPOs have also been effectively used for generation of mid-IR frequency combs [4, 8].

Miniaturizing OPOs has been highly desired for many applications with recent progress in on-chip OPOs based on Kerr [5, 6] and quadratic [17] nonlinearities as well as whispering-gallery resonators [18]. The size of these resonators are still orders of magnitude larger than their operation wavelengths. On the other hand, strong field confinement inside nanostructures has shed light on the possibility of nonlinear optics at nano-scale [19–24]. However, the main focus so far has been devoted to up-conversion in nanostructures and optical parametric oscillation in wavelength-scale structures is still unexplored. The conventional theories which have mostly been developed for travelling wave nonlinear optical systems cannot be directly applied to accurately model

OPOs in nano-structures. The reason is that the spatial variation of the field happens in sub-wavelength scale where slowly-varying envelope approximation (SVEA) is not valid anymore [25]. Moreover, unlike the conventional large-scale OPOs, in nano-structured resonators, the input pump can excite several modes of the cavity at the pump wavelength and it can also directly interact with several modes at the signal wavelength. Few theoretical models have been proposed recently to explain the spontaneous down-conversion in Mie resonators [26] and the threshold in 2D materials-based OPOs [27]. However, these theories are either limited to specific structures or cannot explain the behavior of the system above the threshold.

Here, we derive general conditions to surpass the threshold in wavelength-scale OPOs operating at degeneracy. We show that due to the nonlinear interaction between the pump and the signal modes, the field envelopes slowly evolve/decay in time. In the low-Q regime of wavelength-scale resonators, multiple modes at the signal wavelength can spectrally and spatially overlap (Fig. 1). This allows them to nonlinearly interact with each other through the pump. As an example, we estimate the OPO threshold in an AlGaAs nanoparticle which supports Mie-type multipolar resonances. We show that the multi-mode interaction at signal wavelength can lead to a significant reduction in the threshold by a factor which is remarkably higher than the number of modes. We compare the electric modes versus the magnetic modes, and we show that although the magnetic modes have a higher Q factor, the field overlap can be stronger for the electric modes and as a result, the threshold can be lower for those modes. We establish a connection between up-conversion processes in nanostructures and parametric down-conversion. This allows us to explore the possibility of OPO in the existing structures which have been offered

* marandi@caltech.edu

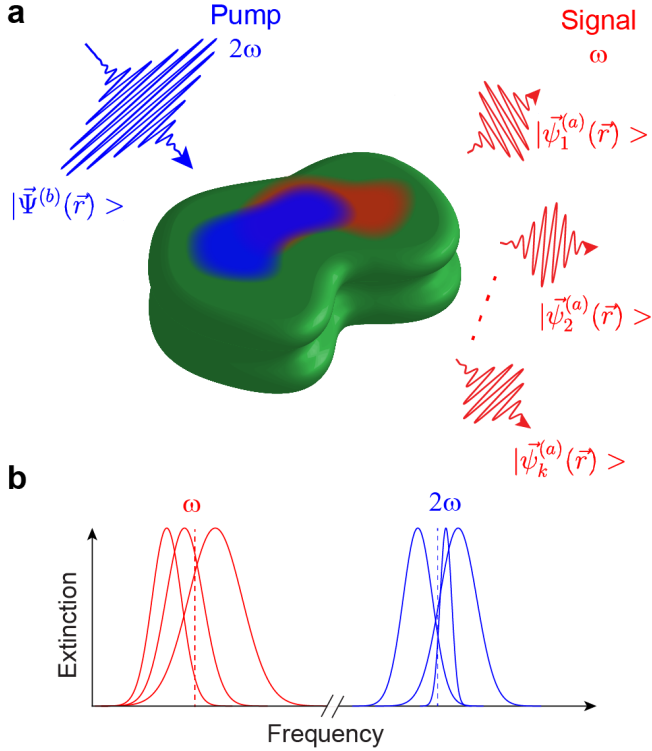


Figure 1. **Wavelength-scale optical parametric oscillators (OPOs).** **a**, An OPO with arbitrary geometry which resonates around the pump frequency (2ω) and the half-harmonic (ω). **b**, The nonlinear behavior of the OPO can be determined by knowing the spatial overlap between the pump excitation at 2ω and eigenmodes of the cavity at ω as well as the linear properties of the cavity around the pump and signal frequencies.

for sum-frequency/second-harmonic generation. Our approach is general and can predict optical parametric oscillation in a wide range of nanostructured resonators, such as bound state in continuum, photonic crystal, and inversely designed cavities.

II. THEORY

To estimate the OPO threshold in multi-mode wavelength-scale resonators, we expand the field in cavity to orthogonal eigenmodes (Fig. 1a), and we approximate the nonlinear dynamics of the electric field with a slowly varying envelope evolving in time-domain (see the Supplementary Material for more details). The electric field for the signal, idler, and pump can be expanded as the superposition of the eigenmodes as $\vec{E}(\vec{r}, t) = \mathcal{E}_a \sum_k a_k(t) e^{-i(\omega - i\frac{\alpha_k}{2})t} |\vec{\psi}_k(\vec{r})\rangle$, where a_k is the slowly varying envelope [28–30], \mathcal{E}_a is the normalization constant such that $|a_k|^2$ is the energy stored in the k^{th} mode of the cavity, and for a homogeneous resonator, it is $\mathcal{E}_a = \sqrt{2/\varepsilon_0 n(\omega)^2}$, $|\vec{\psi}_k(\vec{r})\rangle$ is the cavity eigenmode

normalized such that $\langle \vec{\psi}_m(\vec{r}) | \vec{\psi}_k(\vec{r}) \rangle = \delta_{mk}$ (δ_{mk} is the Kronecker delta), ω is the angular frequency of the signal (ω_s), idler (ω_i) or pump (ω_p), $\alpha_k = \omega_k/Q_k$ is the decay rate of the cavity mode, ω_k is the eigenfrequency of the k^{th} mode with a quality factor of Q_k .

The wave equation for each of the signal eigenmodes at degeneracy ($\omega_s = \omega_i = \omega_p/2 = \omega$) is simplified to (see the Supplementary Material):

$$\frac{d}{dt} a_l = \left(i\delta\omega_l^{(a)} - \frac{\alpha_l^{(a)}}{2} \right) a_l + ib \sum_k \eta_{lk} a_k^*, \quad (1)$$

where a and b represent signal and pump, respectively and η_{lk} is the nonlinear coupling between the l^{th} mode and the k^{th} mode as:

$$\eta_{lk} = \omega \left\langle \frac{\mathcal{E}_b \chi^{(2)}}{n(\omega)^2} \vec{\psi}_l^{(a)*}(\vec{r}) \vec{\Psi}^{(b)}(\vec{r}) \vec{\psi}_k^{(a)*}(\vec{r}) \right\rangle. \quad (2)$$

Note that the pump mode, $b(t)|\vec{\Psi}^{(b)}(\vec{r})\rangle$, is the superposition of the eigenmodes which is dictated by the input excitation. However, the signal has to be expanded to the normal modes (See the Supplementary Material).

The steady-state response of this equation can be written in a matrix form as:

$$\mathcal{M}(b) [a_1, a_1^*, \dots, a_k, a_k^*, \dots]^T = 0. \quad (3)$$

At threshold, the determinant of the matrix \mathcal{M} must be zero to have non-trivial solution for the signal modes. The electric field above threshold can be expressed as a superposition of the eigenmodes as:

$$\vec{E}_\omega(\vec{r}, t) = \sum_m e^{\lambda_m t} \sum_k a_{k,m}^{(a)} |\vec{\psi}_k^{(a)}(\vec{r})\rangle, \quad (4)$$

where $[\lambda_m]$ are the eigenvalues and $\vec{V}_m = [a_{k,m}^{(a)}]$ are the corresponding eigenvectors of \mathcal{M} at threshold which define the signal supermodes. Note that the eigenvalues above threshold must be real to satisfy the phase conjugation in Eq. 1. The minimum pump power to reach this condition defines the oscillation threshold. See the Supplementary Material for more details.

III. RESULTS

Our model is general and can be applied to a wide range of resonators. First, we apply our model to estimate the threshold in an AlGaAs sphere (Fig. 2a). The reason that we have chosen this simple structure is that the eigenmodes for this structure can be derived analytically and be expressed as multipolar resonances [31, 32]. Since the modes for a wide range of nano-structures, such as cylinders and cubes, can be expressed as multipolar resonances as well, our results can shed some light on the possibility of OPO in similar structures which are more amenable to fabrication on a chip [33–40]. Besides,

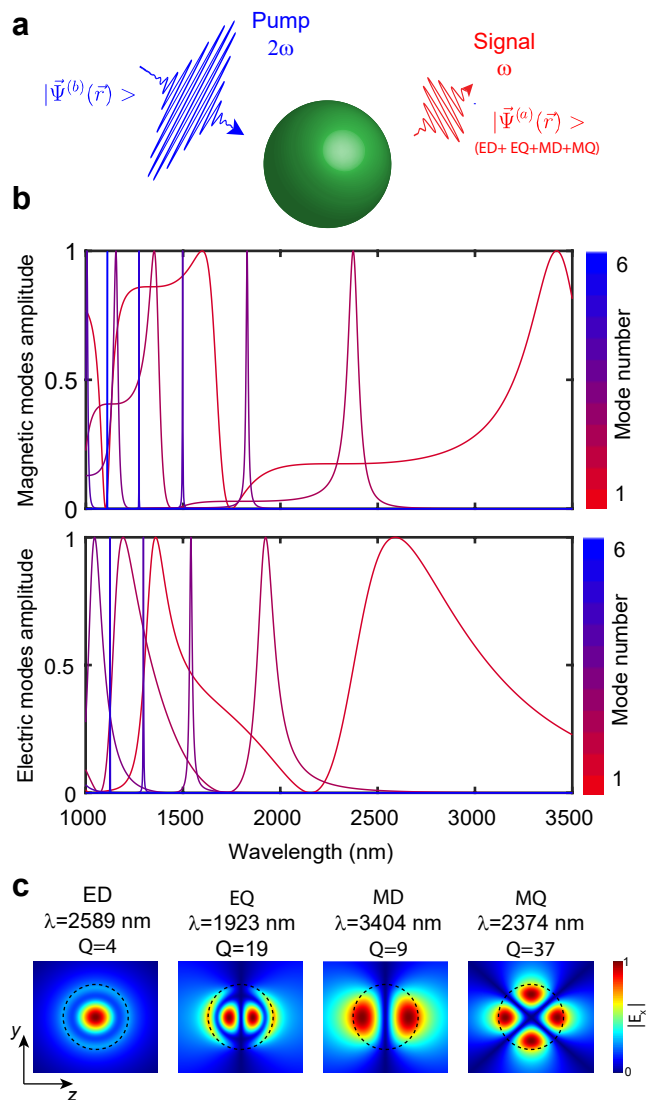


Figure 2. **OPO in a nanoscale dielectric sphere.** **a**, The resonator is composed of a AlGaAs spherical particle with a radius of 500 nm. A pump with a wavelength around the particle size can excite the multipolar modes of the particle. The signal at half-harmonic is the superposition of the lower order modes: electric dipole (ED), electric quadrupole (EQ), magnetic dipole (MD), and magnetic quadrupole (MQ). **b**, Normalized scattering amplitude of the electric and magnetic modes. It is seen that for a broad portion of the spectrum, the particle supports multiple modes which spatially and spectrally overlap. **c**, The normalized x component of the electric field for the first two electric and the first two magnetic eigenmodes. If the pump wavelength is around $1 \mu\text{m}$, the OPO signal can be the superposition of these four modes.

AlGaAs is a low-loss high-index ($\epsilon \approx 10$) material at optical frequencies with strong second-order nonlinearity ($\chi_{ijk}^{(2)} = 200 \text{ pm/V}$, $i \neq j \neq k$) [41], and with appropriate orientation [42], it has been recently explored for strong second-harmonic generation at nanoscale [19, 38–41]. Hence, it is an excellent candidate for demonstration

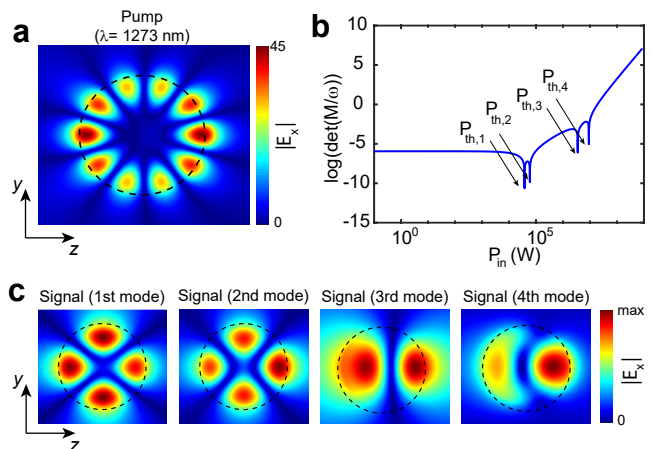


Figure 3. **Degenerate OPO in a dielectric sphere when the pump is resonating.** **a**, The electric field profile at pump wavelength normalized to the input field amplitude. We set the pump wavelength to resonate at the 5^{th} magnetic mode for the particle shown in Fig. 2. The Q-factor for this mode is around 3000. This leads to an enhancement in the electric field intensity inside the particle. **b**, $\det(\mathcal{M}/\omega)$ as a function of the pump power. The pump threshold for parametric oscillation of each supermode at half-harmonic ($\lambda = 2562 \text{ nm}$) is defined as the zeros of $\det(\mathcal{M})$. Since four eigenmodes can be excited at half-harmonic, there are four eigenvalues and four corresponding supermodes. **c**, The electric field profile of the signal supermodes. It is seen that even though the detuning for MQ mode at half-harmonic is significantly larger compared to ED and MD modes, the contribution of MQ mode on the first signal supermode is more evident. This is due to the stronger overlap between the pump mode and the MQ mode. The strong nonlinear coupling between the signal eigenmodes helps to reduce the threshold 50 times compared to the case where we consider only one of the modes for the signal.

of OPO at wavelength-scale with relatively low threshold.

Figure 2b illustrates the normalized scattering coefficients for the first 6 electric and magnetic modes of a particle with a radius of 500 nm. We set the pump wavelength near the particle size ($\approx 1 \mu\text{m}$). If the particle is excited with a plane wave (or a Gaussian beam), several multipolar modes are excited. However, near the resonant wavelength of the higher order modes, due to the high-Q nature of the modes, the excitation is mostly dominated by one mode. At half-harmonic, only the first two electric and the first two magnetic modes can oscillate. The electric field profile of these four modes are illustrated in Fig. 2c. The contribution of each mode in the OPO signal supermode is dictated by the field overlap between the pump and the mode as well as the intermode nonlinear coupling as expressed in Eq. 2, the Q factor, and the detuning from the half-harmonic frequency.

The magnetic modes usually have a higher Q factor compared to the electric modes, and they have been mostly explored for nonlinear wavelength conversion in wavelength-scale dielectric resonators [35]. Hence, we set

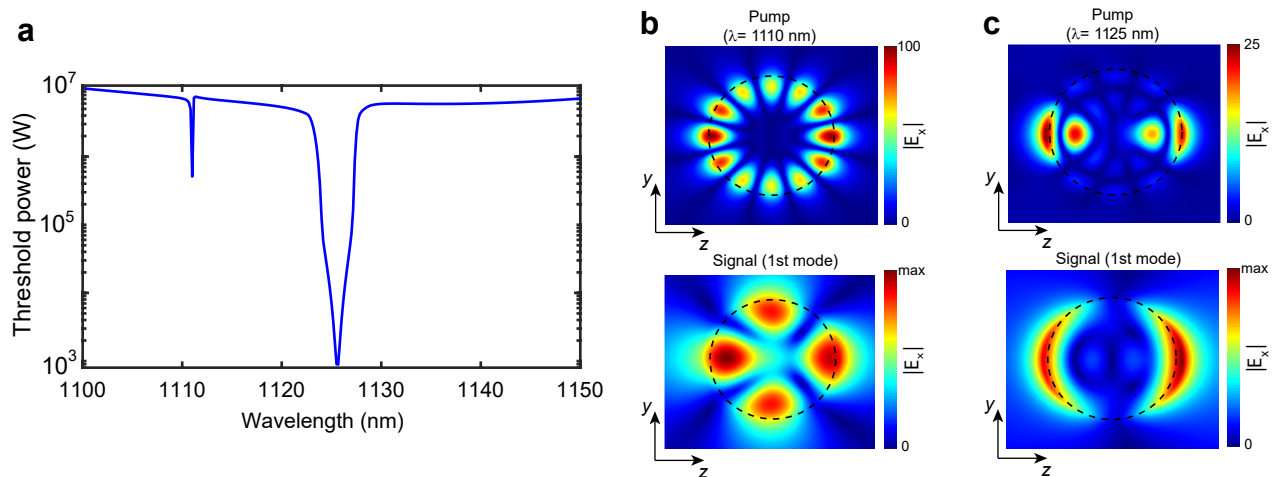


Figure 4. **Magnetic modes versus the electric modes for degenerate OPO.** **a**, The OPO threshold as a function of the pump wavelength. The dips in threshold around 1110 nm and 1125 nm correspond to the 6th magnetic mode and the 5th electric mode, respectively. The Q factor for these modes are 10^4 and 2500, respectively. It is seen that even though the electric mode has a lower Q factor, the threshold is considerably lower. **b**, The electric field distribution for the pump and the first signal supermode when the pump is at $\lambda = 1110$ nm. Due to the large Q, the electric field is remarkably enhanced, but the weak field overlap between the pump and the signal eigenmodes results in a very high threshold. **c**, The electric field distribution for the pump and the first signal supermode when the pump is at $\lambda = 1125$ nm. Because of the strong overlap between the pump and the EQ the threshold is highly reduced.

the wavelength of the pump to coincide with the 5th magnetic mode of the particle. As a result, the field distribution inside the particle is strongly enhanced and dominated by the 5th magnetic mode as shown in Fig. 3a. As seen in Fig. 2b, the signal at half-harmonic dominantly overlaps with the MQ and the ED modes in the spectral domain. The spatial overlap of the pump and the signal modes is represented in the nonlinear coupling term reported in the Supplementary Material.

First, we ignore the intermode coupling and we assume that only one of the eigenmodes can oscillate above the threshold. It is seen that the spatial overlap between the pump and ED, EQ, or MQ (the diagonal terms in η_{lk} matrix) are relatively similar. However, because of the higher Q and lower detuning for MQ mode, the threshold for the MQ mode is the lowest which is 2.23 MW (see the Supplementary Material for the threshold calculations of the other modes and coupling coefficients).

However, when we take the intermode couplings into account, the threshold of the first oscillating mode is reduced almost 50 times as shown in Fig. 3b. In travelling-wave multi-mode OPOs, it is understood that, in the best case scenario, the threshold is of the order of the single-mode threshold divided by the number of modes [43]. The reason is that the modes in travelling wave resonators have the same nature. Thus, the maximum overlap is achieved if all the modes have the same mode profile [43, 44]. However, in wavelength-scale OPOs, each of the multipolar modes have different spatial distribution, and their overlap through the pump field can potentially lead to a strong coupling even higher than the self coupling (the diagonal terms of η_{lk}). The electric field

distribution of the four oscillating supermodes are shown in Fig. 3c. It is seen that the first oscillating mode is mostly dominated by the MQ mode with some contribution from the other modes. The eigenvectors for all four supermodes are reported in the Supplementary Material.

The OPO threshold is inversely proportional to the Q factor of the pump mode if only one mode exists at the pump frequency (see the Supplementary Material). Hence, it is expected to reduce the threshold further by exciting the higher order modes as the higher order multipolar modes have even higher Q factor. Figure 4a shows the OPO threshold for the first supermode as a function of the pump wavelength around the 6th magnetic mode ($\lambda = 1110$ nm) with a Q factor of 10^4 and the 5th electric mode ($\lambda = 1125$ nm) with a Q factor of 2500. It is seen that even though the electric mode has a lower Q factor, the threshold is remarkably lower compared to the adjacent magnetic mode. The electric field distribution for the pump and the first signal supermode for the magnetic and electric mode excitations are shown in Fig. 4b and 4c, respectively. It is seen that the electric field of the magnetic field is significantly enhanced, however, the relatively weak overlap between the pump and the signal eigenmodes has led to a higher threshold compared to the electric mode for which there is a strong overlap between the pump and the EQ mode.

The approach that we used for the calculation of the threshold can also be applied to estimate the second-harmonic generation in multi-mode wavelength-scale resonators (see the Supplementary Material for more details). Specifically, if both pump and signal are single mode and the detuning from the eigenfrequencies is neg-

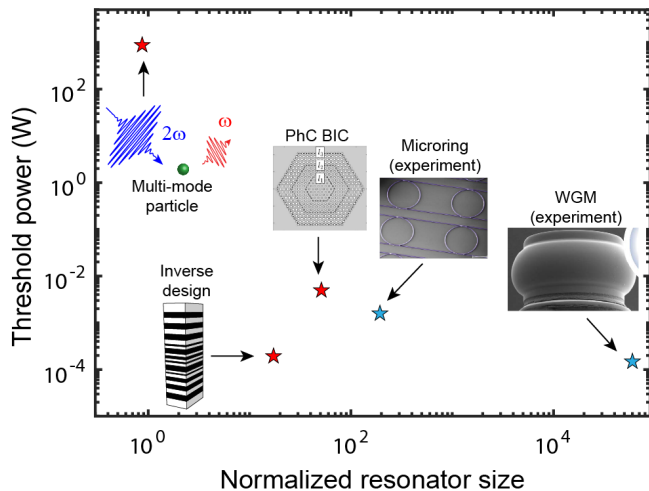


Figure 5. **Estimation of OPO threshold in various platforms.** The estimation of the threshold in a single-mode photonic crystal [45] and inversely designed cavities [46] are based on the reported value for the SHG efficiency. The resonator sizes are normalized to the pump wavelength. As a reference, we have included OPOs demonstrated experimentally based on microring [17] and whispering-gallery mode (WGM) [18] resonators.

ligible, the OPO threshold, and the second-harmonic generation efficiency, ϵ_{SHG} , can be connected as:

$$P_{\text{th}} = \frac{4\alpha^{(a)2}}{\alpha^{(b)2}\epsilon_{\text{SHG}}} \left(\frac{\alpha^{(b)2}}{4} + \delta\omega^{(b)2} \right) \approx \frac{4}{\epsilon_{\text{SHG}}}. \quad (5)$$

As there is no threshold for SHG process and the conventional detectors are more sensitive at shorter wavelengths [47], it is usually easier to simulate or measure the SHG process. This allows us to estimate the OPO threshold in some structures which have been already proposed for SHG. Figure 5 displays few examples and the estimated threshold in these structures. The low threshold in inversely designed structure [46] shows the importance of the field overlap to achieve strong nonlinear response. Note that the thresholds reported in Fig. 5 is for a continuous wave sources.

Since the round-trip time in wavelength-scale OPOs is only few femto-seconds and the Q factor compared to micro-resonators is relatively low, the input pump can be compressed in time into a short pulse. This can help to reduce the threshold in wavelength-scale OPOs to several tens of milliwatts (with a pulse repetition rate of 100 MHz), which is in the order of the threshold for free-space pulsed OPOs [4, 8]. Hence, the oscillation can happen before the onset of the material damage threshold. The field overlap can be further enhanced by Mie resonance engineering, inverse design [48], using hybrid plasmonic structures [22], or controlling evanescent waves [49]. This can potentially help to achieve sub-milliwatt oscillation threshold in wavelength-scale resonators.

IV. CONCLUSION

In conclusion, we proposed a general theory to estimate the threshold in wavelength-scale OPOs operating at degeneracy. We showed that the nonlinear interaction in multi-mode wavelength-scale resonators can be different from their large-scale counterparts and the threshold can be considerably reduced as a result of multimode interaction in these resonators. We showed that although the phase matching is not required in this regime, the field overlap between modes can play a more crucial role compared to increasing the Q factor of the cavity modes. Our formalism is general and can predict the behavior of OPO above the threshold if the pump depletion is also taken into account. It can also be applied to non-degenerate OPOs or $\chi^{(3)}$ cavities. Our approach can enable design of a new class of nonlinear integrated photonic systems.

Wavelength-scale Optical Parametric Oscillator: Supplementary Material

Saman Jahani, Arkadev Roy, and Alireza Marandi

Department of Electrical Engineering, California Institute of Technology, Pasadena, CA 91125, USA.

WAVE EQUATIONS

The Helmholtz wave equation in presence of nonlinear polarizability can be written as:

$$\begin{aligned} \nabla^2 \vec{E} &= \mu_0 \frac{\partial}{\partial t} \left(\frac{\partial \vec{D}}{\partial t} + \sigma \vec{E} \right) \\ &= \mu_0 \varepsilon_0 \varepsilon \frac{\partial^2 \vec{E}}{\partial t^2} + \mu_0 \sigma \frac{\partial \vec{E}}{\partial t} + \mu_0 \frac{\partial^2 \vec{P}_{\text{NL}}}{\partial t^2}, \end{aligned} \quad (6)$$

where $\varepsilon = n^2$ is the linear relative permittivity, n is the refractive index, and P_{NL} is the nonlinear polarization. To find the nonlinear dynamic in wavelength-scale cavities, we write the electric field as a superposition of the cavity eigenmodes. Instead of the conventional form of spatial SVEA in which the envelope evolves as the wave propagates through the nonlinear medium, we assume that the envelope is stationary in space but slowly evolves in time:

$$\begin{aligned} \vec{E}(\vec{r}, t) &= \mathcal{E}_a \sum_k a_k(t) e^{-i(\omega - i\frac{\alpha_k}{2})t} |\vec{\psi}_k(\vec{r})\rangle, \\ \vec{P}_{\text{NL}}(\vec{r}, t) &= \sum_k \vec{P}_k(\vec{r}, t) e^{-i(\omega - i\frac{\alpha_k}{2})t}, \end{aligned} \quad (7)$$

where \mathcal{E}_a is the normalization constant such that $|a_k|^2$ is the energy stored in the k -th mode of the cavity, and for a homogeneous resonator, it is $\mathcal{E}_a = \sqrt{2/\varepsilon_0 n(\omega)^2}$, \vec{P}_k is the nonlinear polarization that we explain later, $|\vec{\psi}_k(\vec{r})\rangle$ is the cavity eigenmode normalized such that $\langle \vec{\psi}_m(\vec{r}) | \vec{\psi}_k(\vec{r}) \rangle = \delta_{mk}$ (δ_{mk} is the Kronecker delta), ω is the angular frequency of the signal, idler or pump, $\alpha_k = \omega_k/Q_k$ is the decay rate of the cavity mode, ω_k is the eigenfrequency of the k -th mode with a quality factor of Q_k .

In the following, we first formulate the nonlinear dynamic for a single-mode OPO at degeneracy, and then we expand the formalism to a multi-mode cavity.

By inserting Eq. 7 in to Eq. 6, considering the k -th mode is the only mode at the operating frequency, we have:

$$\begin{aligned} \left\{ \nabla^2 + \frac{\omega^2}{c^2} n^2 - \frac{n^2}{c^2} \frac{\partial^2}{\partial t^2} + \frac{2i(\omega - i\frac{\alpha_k}{2})}{c^2} n^2 \frac{\partial}{\partial t} \right. \\ \left. + \frac{i\alpha_k \omega - \alpha_k^2/4}{c^2} n^2 + i\omega \mu_0 \sigma + \mu_0 \sigma \frac{\partial}{\partial t} \right\} \mathcal{E}_a a_k(t) |\vec{\psi}_k(\vec{r})\rangle \\ = -\mu_0 \left(\omega - i\frac{\alpha_k}{2} \right)^2 \vec{P}_k + 2i\mu_0 \left(\omega - i\frac{\alpha_k}{2} \right) \frac{\partial \vec{P}_k}{\partial t} + \mu_0 \frac{\partial^2 \vec{P}_k}{\partial t^2}. \end{aligned} \quad (8)$$

Because of SVEA, $\omega \gg \alpha_k$, $\omega P_k \gg \frac{\partial P_k}{\partial t}$, and $\omega a_k \gg \frac{\partial a_k}{\partial t}$. Also, if we ignore the effect of the nonlinearity on the dispersion and if we assume that $\omega = \omega_k + \delta\omega_k$ where $\omega_k \gg \delta\omega_k$, we can assume $\left(\nabla^2 + \frac{\omega_k^2}{c^2} n^2 \right) |\vec{\psi}_k(\vec{r})\rangle \approx 0$. With these approximations, the wave equation is simplified to:

$$\begin{aligned} \left\{ \frac{2i\omega n^2}{c^2} \frac{\partial}{\partial t} + i\omega \mu_0 \sigma a_k \right. \\ \left. + \frac{(2\delta\omega_k + i\alpha_k)\omega n^2}{c^2} \right\} \mathcal{E}_a a_k(t) |\vec{\psi}_k(\vec{r})\rangle = -\mu_0 \omega^2 \vec{P}_k. \end{aligned} \quad (9)$$

Dividing the both sides by $2i\omega n^2/c^2$, we reach:

$$\left\{ \frac{\partial}{\partial t} + \frac{\mu_0 \sigma c^2}{2} - i\delta\omega_k + \frac{\alpha_k}{2} \right\} \mathcal{E}_a a_k(t) |\vec{\psi}_k(\vec{r})\rangle = \frac{i\mu_0 \omega c^2}{2n^2} \vec{P}_k. \quad (10)$$

We first implement the nonlinear dynamics to estimate the threshold in single-mode OPOs. Then, we extend our model when the cavity has multiple modes at the signal wavelength. We also applies our model for second-harmonic generation, we show that if the second-harmonic signal is single-mode, we can estimate the threshold from SHG efficiency. This can be helpful to estimate the OPO threshold for the structures which have already been proposed for SHG.

HALF-HARMONIC GENERATION

By writing the nonlinear polarization, we can find the nonlinear dynamics for different nonlinear processes (e.g. second-harmonic generation and half-harmonic generation). Here, we focus on the threshold for half-harmonic generation in degenerate OPOs. For simplicity, we ignore the ohmic loss of the modes.

The coupled nonlinear wave equation for signal and pump can be written as:

$$\sum_k \left\{ \frac{\partial}{\partial t} - i\delta\omega_k^{(a)} + \frac{\alpha_k^{(a)}}{2} \right\} a_k(t) |\vec{\psi}_k^{(a)}(\vec{r})\rangle \quad (11)$$

$$= \sum_k \frac{i\omega}{2n(\omega)^2} \chi^{(2)}(2\omega, \omega, \omega) \mathcal{E}_b b(t) a_k^*(t) |\vec{\Psi}^{(b)}(\vec{r})\rangle |\vec{\psi}_k^{(a)*}(\vec{r})\rangle,$$

$$\left\{ \frac{\partial}{\partial t} - i\delta\omega^{(b)} + \frac{\alpha^{(b)}}{2} \right\} b(t) |\vec{\Psi}^{(b)}(\vec{r})\rangle \quad (12)$$

$$= \sum_k \frac{i\omega}{n(2\omega)^2} \chi^{(2)}(2\omega, \omega, \omega) \frac{\mathcal{E}_a^2}{\mathcal{E}_b} a_k^2(t) |\vec{\psi}_k^{(a)2}(\vec{r})\rangle.$$

We have defined the electric field for the signal at the fundamental harmonic as $\vec{E}_\omega = \mathcal{E}_a \sum a_k(t) e^{-i(\omega - i\frac{1}{2}\alpha_k^{(a)})t} |\vec{\psi}_k^{(a)}(\vec{r})\rangle$, where $|\vec{\psi}_k^{(a)}(\vec{r})\rangle$ are the eigenmodes of the cavity at $\omega = \omega_k$ with decay constant of $\alpha_k^{(a)}$. The electric field for the pump at second-harmonic is defined as $\vec{E}_{2\omega} = \mathcal{E}_b e^{-i(2\omega - \frac{1}{2}\alpha^{(b)})t} b(t) |\vec{\Psi}^{(b)}(\vec{r})\rangle$, where $|\vec{\Psi}^{(b)}(\vec{r})\rangle$ is the spatial mode profile of the pump normalized such that $\langle \vec{\Psi}^{(b)}(\vec{r}) | \vec{\Psi}^{(b)}(\vec{r}) \rangle = 1$ but, as we explain later, it does not have to be the eigenmode of the cavity and it can be an embedded eigenmode of the cavity, such as Fano, anapole, or bound-state in the continuum modes, $b(t)$ is the envelope of the pump such that $|b|^2$ is the pump power, and $\alpha^{(b)}$ is the decay rate for the pump mode.

A. Single-mode cavity

If $|\vec{\psi}_k^{(a)}(\vec{r})\rangle$ is the only mode of the cavity at the operating frequency, by multiplying the both sides of Eqs. 11 and 12 by $\langle \vec{\psi}_k^{(a)}(\vec{r}) |$ and $\langle \vec{\Psi}^{(b)}(\vec{r}) |$, respectively, and calculating the inner product, the coupled equations are simplified to:

$$\frac{d}{dt} a_k = \left(i\delta\omega_k^{(a)} - \frac{\alpha_k^{(a)}}{2} \right) a_k + i\eta_{kk} b a_k^*, \quad (13)$$

$$\frac{d}{dt} b = \left(i\delta\omega^{(b)} - \frac{\alpha^{(b)}}{2} \right) (b - b_0) + i2\eta_{kk}^* a_k^2, \quad (14)$$

where b_0 is the pump amplitude in the absence of the nonlinearity and η_{kk} is the effective nonlinear coupling defined as:

$$\eta_{kk} = \omega \langle \frac{\mathcal{E}_b \chi^{(2)}}{n(\omega)^2} \vec{\psi}_l^{(a)*}(\vec{r}) \vec{\Psi}^{(b)}(\vec{r}) \vec{\psi}_k^{(a)*}(\vec{r}) \rangle. \quad (15)$$

Near the OPO threshold, we can assume that the pump is not depleted ($b = b_0$). Above threshold, Eqs. 13 and 14 must be solved simultaneously. The steady-state amplitude of the signal is the solution of Eq. 13 when $da_k/dt = 0$. There are two solutions: one of them is the trivial solution, $a_k = 0$, which represents the OPO below the threshold; the nontrivial solution which represents the OPO at threshold. This requires that the amplitude and phase of the pump satisfy these conditions:

$$|\eta_{kk} b_0| \sin(\phi_b - 2\phi_k) = \frac{\alpha_k^{(a)}}{2}, \quad (16)$$

$$|\eta_{kk} b_0| \cos(\phi_b - 2\phi_k) = -\delta\omega_k^{(a)},$$

where ϕ_k and ϕ_b are the phase of the signal mode and the pump mode, respectively. As far as the threshold power is concerned, the above equation can be written in a more compact form [28, 30]:

$$|b_0|^2 = \frac{1}{|\eta_{kk}|^2} \left(\frac{\alpha_k^{(a)2}}{4} + \delta\omega_k^{(a)2} \right). \quad (17)$$

If there is only one coupling channel between the input source and the cavity mode at the pump frequency, in the weak coupling regime ($Q_k \gg 1$), the coupling between the input source and the pump cavity mode in the steady-state can be written as [30]:

$$|b_0|^2 = \frac{\alpha^{(b)}}{\frac{\alpha^{(b)2}}{4} + \delta\omega^{(b)2}} P_{\text{in}}. \quad (18)$$

Hence, the threshold for the input source to go above threshold is:

$$P_{\text{th}} = \frac{1}{\alpha^{(b)} |\eta_{kk}|^2} \left(\frac{\alpha_k^{(a)2}}{4} + \delta\omega_k^{(a)2} \right) \left(\frac{\alpha^{(b)2}}{4} + \delta\omega^{(b)2} \right). \quad (19)$$

If there are more than one coupling channel between the input and the cavity, such as the excitation from the free-space, Eq. 19 is not accurate, and the coupling between the input power and the pump mode amplitude, b_0 , should be derived from the linear analysis of the cavity at the pump frequency.

B. Multi-mode cavity

For wavelength-scale cavities, the quality factor of the modes are usually low. Hence, at operating wavelength more than one can resonate. If the cavity is multi-mode at the operating wavelength, by multiplying the both sides of Eq. 11 by $\langle \vec{\psi}_l^{(a)}(\vec{r}) |$, the coupled equation is simplified to:

$$\frac{d}{dt} a_l = \left(i\delta\omega_l^{(a)} - \frac{\alpha_l^{(a)}}{2} \right) a_l + i b \sum_k \eta_{lk} a_k^*. \quad (20)$$

The steady-state response of this equation can be written in a matrix form as:

$$\mathcal{M}(b) [a_1, a_1^*, \dots, a_k, a_k^*, \dots]^T = 0. \quad (21)$$

At threshold, the determinant of the matrix \mathcal{M} must be zero to have non-trivial solution for the signal modes.

$$\vec{E}_\omega(\vec{r}, t) = \sum_m e^{\lambda_m t} \sum_k a_{k,m}^{(a)} |\vec{\psi}_k^{(a)}(\vec{r})\rangle, \quad (22)$$

where $[\lambda_m]$ are the eigenvalues and $[a_{k,m}^{(a)}]$ are the corresponding eigenvectors of \mathcal{M} at threshold, which must be real to satisfy the phase conjugation in Eq. 20. The OPO threshold is the minimum pump power for which the largest eigenvalue of the matrix surpasses zero. Near the threshold, that is the only oscillating mode and the eigenvector correspond to that eigenvector describes the spatial distribution of the signal. The phase difference between each mode of the pulse and the pump is set automatically to achieve the minimum threshold. There is

no closed form solution for the eigenvalue if the quality factors of the modes or the central frequencies of all modes are not the same. However, in the best case scenario where all the modes have similar nonlinear coupling coefficient and quality factor, the threshold is reduced by a factor which is the number of modes.

SECOND-HARMONIC GENERATION

We can implement the same approach for calculating the SHG in cavities. However, for SHG, we have to expand the second-harmonic mode into the eigenmodes of the cavity while the pump input at fundamental harmonic can be an embedded mode of the cavity. If we ignore the back conversion, the nonlinear dynamic for SHG process can be written as:

$$\begin{aligned} \sum_k \left\{ \frac{\partial}{\partial t} - i\delta\omega^{(b_k)} + \frac{\alpha_k^{(b)}}{2} \right\} b_k(t) |\psi_k^{(b)}(\vec{r})\rangle & \quad (23) \\ = \frac{i\omega}{n^2} \chi^{(2)}(2\omega, \omega, \omega) a^2(t) |\vec{\Psi}^{(a)}(\vec{r})\rangle^2. \end{aligned}$$

By multiplying the both sides by $\langle \psi_k^{(b)} |$. Eq. 23 is simplified to:

$$\frac{d}{dt} b_k = \left(i\delta\omega_k^{(b)} - \frac{\alpha_k^{(b)}}{2} \right) b_k + i2\tilde{\eta}_k^* a^2, \quad (24)$$

where $\tilde{\eta}_k = \omega \langle \mathcal{E} \frac{\chi^{(2)}}{n^2} \vec{\Psi}^{(a)*}(\vec{r})^2 \psi_k^{(b)}(\vec{r}) \rangle$. If we assume that the pump is constant ($a(t) = a_0$), the steady-state second-harmonic generated power is:

$$|b_k|^2 = \frac{4\tilde{\eta}_k^2}{\frac{\alpha_k^{(b)2}}{4} + \delta\omega_k^{(b)2}} |a_0|^4 \quad (25)$$

If there is only one coupling channel between the input and the cavity mode at the fundamental frequency, the cavity mode amplitude can be written as the input power as:

$$\begin{aligned} |a_0|^2 &= \frac{\alpha^{(a)}}{\frac{\alpha^{(a)2}}{4} + \delta\omega^{(a)2}} P_{\text{in}}, & (26) \\ |b_k|^2 &= \frac{\alpha_k^{(b)}}{\frac{\alpha_k^{(b)2}}{4} + \delta\omega_k^{(b)2}} P_{\text{SHG},k}. \end{aligned}$$

By inserting Eq. 26 in to Eq. 25, the second-harmonic power can be expressed as $P_{\text{SHG},k} = \epsilon_{\text{SHG},k} P_{\text{in}}^2$, where ϵ_{SHG} is the SHG efficiency in the unit of W^{-1} written as:

$$\epsilon_{\text{SHG},k} = \frac{4\tilde{\eta}_k^2 \alpha^{(a)2}}{\alpha_k^{(b)} \left(\frac{\alpha^{(a)2}}{4} + \delta\omega^{(a)2} \right)^2}. \quad (27)$$

If the cavity is single mode at both the fundamental and second harmonic, $\tilde{\eta}_k = \eta_{kk}$. This allows us to connect the SHG efficiency to the nonlinear coupling coefficient. Hence, by knowing the linear response of the cavity and SHG efficiency, we can derive the OPO threshold by inserting Eq. 27 into Eq. 19:

$$P_{\text{th}} = \frac{4\alpha^{(a)2}}{\alpha^{(b)2} \epsilon_{\text{SHG}}} \left(\frac{\alpha^{(b)2}}{4} + \delta\omega^{(b)2} \right) \approx \frac{4}{\epsilon_{\text{SHG}}}. \quad (28)$$

OPO IN SPHERICAL DIELECTRIC PARTICLE

The nonlinear coupling (Eq. 15) for the particle in Fig. 3 in the main text is calculated as:

$$|\eta_{lk}| = 10^{10} \times \begin{bmatrix} 0.1695 & 0.3295 & 0.2712 & 0.2460 \\ 0.3295 & 0.2082 & 0.3362 & 1.9519 \\ 0.2712 & 0.3362 & 0.0466 & 0.4945 \\ 0.2460 & 1.9519 & 0.4945 & 0.1338 \end{bmatrix} \quad (29)$$

The modes are ordered as: ED, EQ, MD, and MQ. If we ignore intermode coupling, the threshold for these modes are: 3.92, 17.94, 219.76, and 2.23 MW, respectively. However, due to the strong intermode coupling, especially between EQ and MQ, the threshold is reduced 50-fold as shown in Fig. 3 in the main text. The supermodes are the eigenvectors of $\mathcal{M}(b)$ at thresholds, which are calculated as:

$$\begin{aligned} |\vec{V}_1| &= [0.0260 \quad 0.0120 \quad 0.0350 \quad 0.6297] & (30) \\ |\vec{V}_2| &= [0.0433 \quad 0.0391 \quad 0.0507 \quad 0.6073] \\ |\vec{V}_3| &= [0.0756 \quad 0.3891 \quad 0.5942 \quad 0.1184] \\ |\vec{V}_4| &= [0.0369 \quad 0.4674 \quad 0.4829 \quad 0.1605] \end{aligned}$$

-
- [1] R. C. Eckardt, C. Nabors, W. J. Kozlovsky, and R. L. Byer, *JOSA B* **8**, 646 (1991).
[2] A. Schliesser, N. Picqué, and T. W. Hänsch, *Nature Photonics* **6**, 440 (2012).
[3] I. Breunig, *Laser & Photonics Reviews* **10**, 569 (2016).
[4] A. Marandi, N. C. Leindecker, V. Pervak, R. L. Byer, and K. L. Vodopyanov, *Optics express* **20**, 7255 (2012).
[5] T. Kippenberg, S. Spillane, and K. Vahala, *Physical review letters* **93**, 083904 (2004).
[6] Y. Okawachi, M. Yu, K. Luke, D. O. Carvalho, S. Ramelow, A. Farsi, M. Lipson, and A. L. Gaeta, *Optics letters* **40**, 5267 (2015).
[7] T. Inagaki, K. Inaba, R. Hamerly, K. Inoue, Y. Yamamoto, and H. Takesue, *Nature Photonics* **10**, 415

- (2016).
- [8] A. Muraviev, V. Smolski, Z. Loparo, and K. Vodopyanov, *Nature Photonics* **12**, 209 (2018).
- [9] J. Roslund, R. M. De Araujo, S. Jiang, C. Fabre, and N. Treps, *Nature Photonics* **8**, 109 (2014).
- [10] G. Milburn and D. Walls, *Optics Communications* **39**, 401 (1981).
- [11] L.-A. Wu, H. J. Kimble, J. L. Hall, and H. Wu, *Physical review letters* **57**, 2520 (1986).
- [12] M. Chen, N. C. Menicucci, and O. Pfister, *Physical review letters* **112**, 120505 (2014).
- [13] O. Morin, K. Huang, J. Liu, H. Le Jeannic, C. Fabre, and J. Laurat, *Nature Photonics* **8**, 570 (2014).
- [14] R. Nehra, A. Win, M. Eaton, R. Shahrokhshahi, N. Sridhar, T. Gerrits, A. Lita, S. W. Nam, and O. Pfister, *Optica* **6**, 1356 (2019).
- [15] A. Marandi, Z. Wang, K. Takata, R. L. Byer, and Y. Yamamoto, *Nature Photonics* **8**, 937 (2014).
- [16] P. L. McMahon, A. Marandi, Y. Haribara, R. Hamerly, C. Langrock, S. Tamate, T. Inagaki, H. Takesue, S. Utsunomiya, K. Aihara, *et al.*, *Science* **354**, 614 (2016).
- [17] A. W. Bruch, X. Liu, J. B. Surya, C.-L. Zou, and H. X. Tang, *Optica* **6**, 1361 (2019).
- [18] C. S. Werner, T. Beckmann, K. Buse, and I. Breunig, *Optics letters* **37**, 4224 (2012).
- [19] D. Smirnova and Y. S. Kivshar, *Optica* **3**, 1241 (2016).
- [20] S. Jahani and Z. Jacob, *Optica* **1**, 96 (2014).
- [21] F. Monticone and A. Alu, *Physical Review Letters* **112**, 213903 (2014).
- [22] M. P. Nielsen, X. Shi, P. Dichtl, S. A. Maier, and R. F. Oulton, *Science* **358**, 1179 (2017).
- [23] O. Reshef, I. De Leon, M. Z. Alam, and R. W. Boyd, *Nature Reviews Materials* **4**, 535 (2019).
- [24] Y. Yang, J. Lu, A. Manjavacas, T. S. Luk, H. Liu, K. Kelley, J.-P. Maria, E. L. Runnerstrom, M. B. Sinclair, S. Ghimire, *et al.*, *Nature Physics* **15**, 1022 (2019).
- [25] R. Hamerly, A. Marandi, M. Jankowski, M. M. Fejer, Y. Yamamoto, and H. Mabuchi, *Physical Review A* **94**, 063809 (2016).
- [26] A. N. Poddubny and D. A. Smirnova, *arXiv preprint arXiv:1808.04811* (2018).
- [27] A. Ciattoni, A. Marini, C. Rizza, and C. Conti, *Light: Science & Applications* **7**, 5 (2018).
- [28] H. A. Haus, *Waves and fields in optoelectronics* (Prentice-Hall, 1984).
- [29] C. Fabre, E. Giacobino, A. Heidmann, L. Lugiato, S. Reynaud, M. Vadacchino, and W. Kaige, *Quantum Optics: Journal of the European Optical Society Part B* **2**, 159 (1990).
- [30] A. Rodriguez, M. Soljačić, J. D. Joannopoulos, and S. G. Johnson, *Optics express* **15**, 7303 (2007).
- [31] S. Jahani and Z. Jacob, *Nature nanotechnology* **11**, 23 (2016).
- [32] A. I. Kuznetsov, A. E. Miroshnichenko, M. L. Brongersma, Y. S. Kivshar, and B. Lukyanchuk, *Science* **354**, aag2472 (2016).
- [33] D. G. Baranov, D. A. Zuev, S. I. Lepeshov, O. V. Kotov, A. E. Krasnok, A. B. Evlyukhin, and B. N. Chichkov, *Optica* **4**, 814 (2017).
- [34] A. Krasnok, M. Tymchenko, and A. Alù, *Materials Today* **21**, 8 (2018).
- [35] T. Pertsch and Y. Kivshar, *MRS Bulletin* **45**, 210 (2020).
- [36] S. Liu, M. B. Sinclair, S. Saravi, G. A. Keeler, Y. Yang, J. Reno, G. M. Peake, F. Setzpfandt, I. Staude, T. Pertsch, *et al.*, *Nano letters* **16**, 5426 (2016).
- [37] L. Carletti, K. Koshelev, C. De Angelis, and Y. Kivshar, *Physical review letters* **121**, 033903 (2018).
- [38] G. Marino, A. S. Solntsev, L. Xu, V. F. Gili, L. Carletti, A. N. Poddubny, M. Rahmani, D. A. Smirnova, H. Chen, A. Lemaître, *et al.*, *Optica* **6**, 1416 (2019).
- [39] M. Timofeeva, L. Lang, F. Timpu, C. Renault, A. Bouravleuv, I. Shtrom, G. Cirlin, and R. Grange, *Nano letters* **18**, 3695 (2018).
- [40] K. Koshelev, S. Kruk, E. Melik-Gaykazyan, J.-H. Choi, A. Bogdanov, H.-G. Park, and Y. Kivshar, *Science* **367**, 288 (2020).
- [41] V. Gili, L. Carletti, A. Locatelli, D. Rocco, M. Finazzi, L. Ghirardini, I. Favero, C. Gomez, A. Lemaître, M. Celebrano, *et al.*, *Optics Express* **24**, 15965 (2016).
- [42] S. Buckley, M. Radulaski, J. L. Zhang, J. Petykiewicz, K. Biermann, and J. Vučković, *Optics express* **22**, 26498 (2014).
- [43] G. J. De Valcarcel, G. Patera, N. Treps, and C. Fabre, *Physical Review A* **74**, 061801 (2006).
- [44] G. Alves, R. Barros, D. Tasca, C. Souza, and A. Khoury, *Physical Review A* **98**, 063825 (2018).
- [45] M. Minkov, D. Gerace, and S. Fan, *Optica* **6**, 1039 (2019).
- [46] Z. Lin, X. Liang, M. Lončar, S. G. Johnson, and A. W. Rodriguez, *Optica* **3**, 233 (2016).
- [47] R. H. Hadfield, *Nature photonics* **3**, 696 (2009).
- [48] S. Molesky, Z. Lin, A. Y. Piggott, W. Jin, J. Vucković, and A. W. Rodriguez, *Nature Photonics* **12**, 659 (2018).
- [49] S. Jahani, S. Kim, J. Atkinson, J. C. Wirth, F. Kalhor, A. Al Noman, W. D. Newman, P. Shekhar, K. Han, V. Van, *et al.*, *Nature communications* **9**, 1 (2018).